Hydrogen and fluorine migration in photo-double-ionization of 1,1-difluoroethylene (1,1-$C_2H_2F_2$) near and above threshold

B. Gaire,[1] I. Bocharova,[1] F. P. Sturm,[1,2] N. Gehrken,[1,2] J. Rist,[1,2] H. Sann,[2] M. Kunitski,[2] J. Williams,[2] M. S. Schöffler,[2] T. Jahnke,[2] B. Berry,[3] M. Zohrabi,[3] M. Keiling,[2,4] A. Moradmand,[4] A. L. Landers,[4] A. Belkacem,[1] R. Dörner,[2] I. Ben-Itzhak,[3] and Th. Weber[1]

[1]*Chemical Sciences Division, Lawrence Berkeley National Laboratory, Berkeley, California 94720, USA*

[2]*Institut für Kernphysik, Goethe-Universität, Max-von-Laue-Str.1, 60438 Frankfurt am Main, Germany*

[3]*J. R. Macdonald Laboratory, Department of Physics, Kansas State University, Manhattan, Kansas 66506, USA*

[4]*Department of Physics, Auburn University, Alabama 36849, USA*

(Received 26 February 2014; published 21 April 2014)

We have studied the nondissociative and dissociative photo-double-ionization of 1,1-difluoroethylene using single photons of energies ranging from 40 to 70 eV. Applying a coincident electron-ion three-dimensional momentum imaging technique, kinematically complete measurements have been achieved. We present the branching ratios of the six reaction channels identified in the experiment. Electron-ion energy maps and relative electron emission angles are used to distinguish between direct and indirect photo-double-ionization mechanisms at a few different photon energies. The influence of selection and propensity rules is discussed. Threshold energies of double ionization are extracted from the sum of the kinetic energies of the electrons, which hint to the involvement of different manifolds of states. The dissociative ionization channels with two ionic fragments are explored in detail by measuring the kinetic energy release of the fragment ions, sum of the kinetic energies, as well as the energy sharing of the two emitted electrons. We investigate the migration of hydrogen and fluorine atoms and compare the experimental results to the photo-double-ionization of centrosymmetric linear and planar hydrocarbons (C_2H_2 and C_2H_4) whenever possible.

DOI: 10.1103/PhysRevA.89.043423 PACS number(s): 33.80.Eh, 33.90.+h

I. INTRODUCTION

Photo-double-ionization (PDI) is a process in which two electrons are removed from an atom or a molecular target with a single photon. Studies of PDI lead to a better understanding of the correlation between the electrons, the ionization mechanisms leading to the ejection of the two electrons, selection and propensity rules prohibiting transitions, and the molecular dynamics during the transition from the neutral ground state to the respective dication or the ionic fragments. The ionization to the dication states can occur either through a direct or an indirect process. In the low-photon-energy regime, the direct process is thought of as a photoabsorption by one electron which then hits another electron on the way out of the target leading to double ionization (sometimes referred to as a two-step-one process, TS1; the time-reversed process of the TS1, which is a pure quantum mechanical effect, is referred to as ground-state correlation, GSC [1]). In the indirect process (sometimes also referred to as a sequential process), photoejection of one electron leads to an intermediate cation state, which later decays by autoionization or other processes (e.g., Auger decay, fluorescence, etc.). After a couple of decades of studying the PDI of simple atoms and diatomic molecules (e.g., He, H_2, N_2, CO) in great detail [2–10], the investigation has been extended to polyatomic molecules in order to gain a general understanding of the double-ionization process in more complex systems. Simple hydrocarbon molecules are an ideal testbed for a series of studies with increasing complexity. Here, we choose the 1,1-difluoroethylene (1,1-$C_2H_2F_2$, $^{H}_{H}$>C=C<$^{F}_{F}$) molecule as a followup to our recent investigation of acetylene (C_2H_2) and ethylene (C_2H_4) [11]. The latter molecules are simple centrosymmetric closed-shell hydrocarbon molecules. The 1,1-$C_2H_2F_2$ molecule is made by substitution of two hydrogen atoms by fluorine atoms on the same side of the C=C bond of C_2H_4. The other two isomers of difluoroethylene are 1,2-cis-$C_2H_2F_2$ ($^{H}_{F}$>C=C<$^{H}_{F}$) and 1,2-trans-$C_2H_2F_2$ ($^{H}_{F}$>C=C<$^{F}_{H}$).

We expect differences in the PDI of the valance electrons of 1,1-$C_2H_2F_2$ as compared to C_2H_4. For example, the propensity rule proposed for the PDI of centrosymmetric molecules [10,12,13], which states that the triplet gerade and singlet ungerade electronic states of the dications are likely to be populated, is no longer valid for 1,1-$C_2H_2F_2$. Hence, the nondissociative ionization (NDI) of these two species can be very different. In addition, a variety of reaction channels can be expected in the dissociative ionization (DI) of 1,1-$C_2H_2F_2$. For instance, in C_2H_4, the migration of H atoms from one side of the C=C double bond to the other simply can not be distinguished (at least in our experiments). In contrast, a migration of atoms from the opposite sides of the double bond in 1,1-$C_2H_2F_2$ leads to distinguishable conformations of the molecule. The symmetric breakup channel of 1,1-$C_2H_2F_2$ leading to two CHF^+ fragment ions, on the other hand, is very complex since it would require multiple bond breaking and a subsequent rearrangement of the constituent atoms, which is obviously not the case for C_2H_4 and C_2H_2 due to their mirror symmetry.

In the past, Ibuki and co-workers explored the PDI of 1,1-$C_2H_2F_2$ and 1,1-$C_2H_2D_2$ in the photon energy range of 37–85 eV using a photoion-photoion coincidence (PIPICO) technique [14]. They measured the branching ratios of the singly charged cations, and they explained the two main

pathways involving the C=C and C-H bond breakup. On the theoretical side, Frenking *et al.* [15] investigated the optimized geometries and energies of the fluorine-substituted ethylene dications using *ab initio* methods. They predicted that the lowest-energy state of the 1,1-$C_2H_2F_2^{2+}$ dication prefers a nonplanar twisted geometry similar to that of $C_2H_4^{2+}$. The second lowest dication state has a planar geometry and is 0.25 eV higher in energy than the ground state. However, when all four hydrogen atoms in the $C_2H_4^{2+}$ dication are replaced by fluorine atoms, the resulting $C_2F_4^{2+}$ dication appears to be more stable in a planar configuration [15,16].

In this work, we report on the PDI of the valence electrons of 1,1-$C_2H_2F_2$ by using different photon energies (40, 50, 60, and 70 eV) of linearly polarized synchrotron light resulting in NDI and various DI channels. We discuss the detection of metastable dications and the variation in their branching ratio as a function of the photon energy. The ionization mechanisms, i.e., the emission of two electrons via direct or indirect ionization processes, are analyzed using electron-ion energy correlation maps, electron energy sharing, and relative electron-electron emission angles, i.e., the angle (θ_{12}) between the momentum vectors of two electrons. Moreover, we present the kinetic energy distributions of the electrons and nuclear fragments for the DI channels we have measured. They provide a wealth of information on the PDI and the subsequent dynamics. In the next section, we briefly describe the experimental method. We then present the results and a discussion.

II. EXPERIMENTAL METHOD

We employ cold target recoil ion momentum spectroscopy (COLTRIMS) [17–19] to study the nondissociative and dissociative ionization of 1,1-difluoroethylene (1,1-$C_2H_2F_2$). Linearly polarized single photons with energies ranging from 40 to 70 eV are provided at the undulator beamline 10.0.1 of the Advanced Light Source (ALS) of the Lawrence Berkeley National Laboratory (LBNL). The light beam orthogonally intersects the supersonic gas jet of target molecules inside our three-dimensional (3D) momentum imaging spectrometer. The electrons generated in the ionization event are guided by a static electric field (17 V/cm) and an axial magnetic field (12 Gauss) into one arm of the spectrometer. The positively charged recoil ions are guided by the same combination of fields into the opposite arm of the spectrometer. The ions and electrons are detected with multihit capable time- and position-sensitive detectors. The static electric field is directed along the axis of the spectrometer (which is parallel to the polarization vector of the light) and is at right angles to both the photon beam and the supersonic gas jet. It is important to note that a full collection angle of 4π (sr) is achieved for both electrons and ions and that they are measured in coincidence.

We use microchannel-plate (MCP) detectors with delay-line anodes [20–22] to record the time-of-flight (TOF) to and the position of impact on the detector of both species (electrons and ions) in an event-mode data-acquisition scheme. From the recorded information, the 3D momentum vectors for each of the charged fragments are retrieved, enabling the realization of kinematically complete experiments (e.g., [17–19]). From these momentum vectors we evaluate the energies and emission angles of the electrons and the fragment ions. The sum of the kinetic energies of the electrons (E_{sum}) subtracted from the photon energy (E_γ) gives the threshold energy of the PDI process, and thus marks the appearance energy on the potential energy surface (PES) of the metastable dications that may or may not fragment. Fragmentation of the dication results in DI channels; otherwise, we detect the NDI channel. The kinetic energy release (KER), which is the sum of the kinetic energies of the nuclear fragments in the center-of-mass frame of the molecule, and the E_{sum} of the photoelectrons are used to track down the most likely fragmentation pathways on the PES [11]. Note that the KER marks the energy difference between the points on the PES where the dissociation begins and the asymptotic limit of the corresponding final state on the same PES or another one if transition(s) occurred.

III. RESULTS AND DISCUSSION

The following six PDI channels of 1,1-difluoroethylene are observed in our measurements at photon energies of 40, 50, 60, and 70 eV:

$$\begin{aligned} C_2H_2F_2 + E_\gamma &\rightarrow C_2H_2F_2^{2+} + 2e^- \quad \text{(NDI)} \\ &\rightarrow H^+ + C_2HF_2^+ + 2e^- \\ &\rightarrow CH_2^+ + CF_2^+ + 2e^- \\ &\rightarrow CF^+ + CH_2F^+ + 2e^- \\ &\rightarrow HF^+ + C_2HF^+ + 2e^- \\ &\rightarrow H_2^+ + C_2F_2^+ + 2e^-, \end{aligned}$$

where E_γ represents the photon energy. The dissociative ionization channels which result in two ionic fragments form narrow stripes in the photoion-photoion coincidence (PIPICO) TOF spectrum shown in Fig. 1.

A. Branching ratios

The relative yield, i.e., the branching ratio, of a particular channel is obtained by integrating the corresponding E_{sum} distribution associated with the respective breakup channel in the PIPICO spectrum while requiring momentum conservation for the recoil ions (i.e., a momentum sum of zero within an uncertainty which is ± 6 a.u. corresponding to 5% to 20% of the ion momentum for the respective breakup channels) as employed in our earlier work on ethylene (C_2H_4) and acetylene (C_2H_2) [11]. The overall branching ratio for each of these channels is presented in Table I and also in Fig. 2 for all photon energies used in our measurements.

Surveying the branching ratios presented in Fig. 2(a), one can see that the branching ratio of each DI channel varies differently with photon energy. Among the DI channels, the yield of the $CF^+ + CH_2F^+$ breakup channel decreases for increasing photon energy. This channel involves a fluorine migration and a subsequent central C=C bond cleavage. The $CH_2^+ + CF_2^+$ channel, which in contrast results from a prompt breakup of the central C=C bond, is dominant at all the photon energies used in our measurements. The branching ratio of the $H^+ + C_2HF_2^+$ channel (also referred to as deprotonation) is almost constant (at about 16%) for all photon energies employed. One can notice that the yield of the $HF^+ + C_2HF^+$

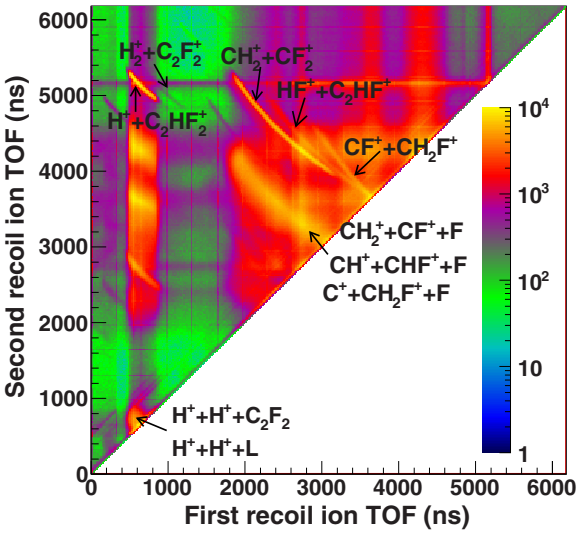

FIG. 1. (Color online) Photoion-photoion coincidence (PIPICO) spectrum used to identify and separate the different breakup channels of the PDI of 1,1-$C_2H_2F_2$ using single photons at 60 eV. The PIPICO spectrum shows the ion-pair yield as function of TOF of the first and the second recoil ion. Channels with two ionic fragments for which we have the kinematically complete information are labeled in the upper half. The breakup channels producing two protons and a neutral fragment ($H^+ + H^+ + C_2F_2$) or two or more neutral or charged ions which are lost in our detection scheme ($H^+ + H^+ + L$) are marked in the lower half. The dominant many-body breakup channels are also marked as $CH_2^+ + CF^+ + F$, $CH^+ + CHF^+ + F$, and $C^+ + CH_2F^+ + F$.

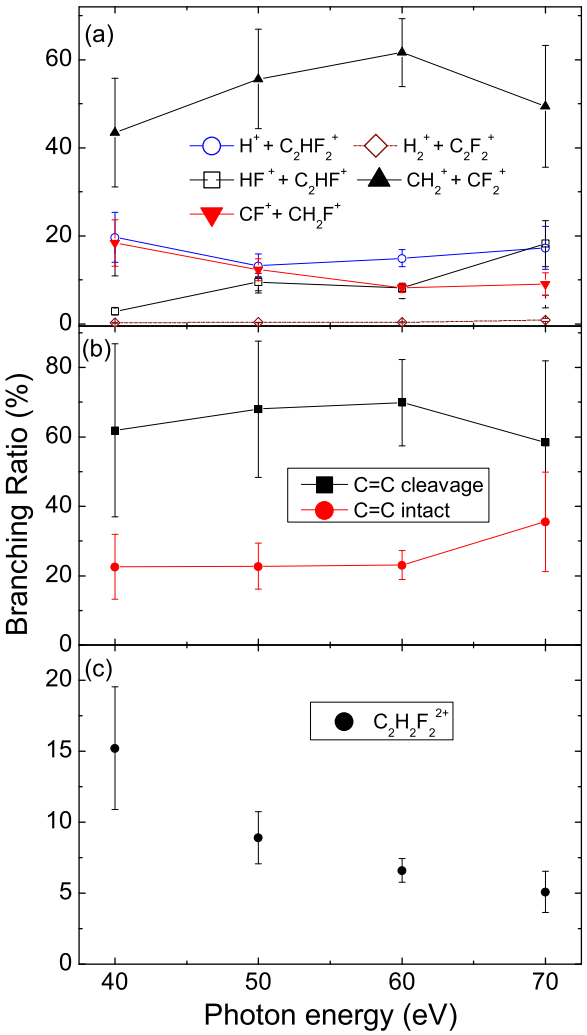

FIG. 2. (Color online) Branching ratios of different channels from the photo-double-ionization of the 1,1-$C_2H_2F_2$ molecules using linearly polarized photons of 40- to 70-eV energy. (a) Branching ratio of different two ionic fragments channels. (b) Sum of the branching ratio of the channels involving the cleavage of the central C=C bond (black solid squares) and rest of the dissociative ionization channels (red solid circles). (c) Branching ratio of the long-lived dications (black solid circles).

channel increases with the photon energy, and this trend is almost the opposite of the $CF^+ + CH_2F^+$ breakup. This is likely related to the progression of the fluorine migration during the dissociation, which is common to both channels, while a hydrogen atom is either migrating simultaneously or not (further discussed below). The $H_2^+ + C_2F_2^+$ channel yield is very low (below 1%) and rather constant on the level observed. We outline the possibility of such a low yield later when the individual DI channels are discussed.

The branching ratio of the NDI channel decreases with increasing photon energy as shown in Fig. 2(c). One of the possibilities for this reduction is that at higher photon energies, excited dication states are populated, which are repulsive and thus dissociate. One can see that the threshold energy distribution presented in Fig. 3 has shoulders at higher energies for DI channels, a fact that supports the increasing role of highly excited states.

TABLE I. Sum of the kinetic energies of electrons (E_{sum}, in eV), kinetic energy release (KER, in eV), and the branching ratio (BR, in %) of NDI and different DI channels following the photo-double-ionization of 1,1-$C_2H_2F_2$ using single photons of 40 to 70 eV energy. The branching ratios are corrected for the overall detection efficiency of different channels by using the estimated detection efficiency of individual ions as mentioned in Ref. [23].

	$E_\gamma = 40$ eV			$E_\gamma = 50$ eV			$E_\gamma = 60$ eV			$E_\gamma = 70$ eV		
Channels	E_{sum}	KER	BR (%)	E_{sum}	KER	BR (%)	E_{sum}	KER	BR (%)	E_{sum}	KER	BR (%)
$C_2H_2F_2^{2+}$	9.4		15.2 ± 4.3	19.5		8.9 ± 1.8	29.5		6.6 ± 0.8	39.0		5.1 ± 1.4
$H^+ + C_2HF_2^+$	5.0	4.5	19.7 ± 5.7	14.0	4.5	13.2 ± 2.7	24.0	4.5	15.0 ± 1.9	33.2	4.5	17.3 ± 4.9
$CH_2^+ + CF_2^+$	6.0	4.5, 5.5	43.5 ± 12.3	15.5	4.5, 5.5	55.6 ± 11.3	25.5	4.5, 5.5	61.6 ± 7.7	34.0	4.5, 5.5	49.4 ± 13.8
$CF^+ + CH_2F^+$	8.0	6.0	18.4 ± 5.3	18.0	6.0	12.3 ± 2.5	28.0	6.0	8.2 ± 1.0	37.0	6.0	9.0 ± 2.6
$HF^+ + C_2HF^+$	6.0	4.1	2.9 ± 0.9	13.5	4.2	9.6 ± 2.0	23.0	4.0	8.2 ± 1.0	33	4.2	18.3 ± 5.2
$H_2^+ + C_2F_2^+$		4.0	0.3 ± 0.1	12.0	4.1	0.4 ± 0.1	22.0	4.0	0.4 ± 0.1	31.0	4.0	0.9 ± 0.3

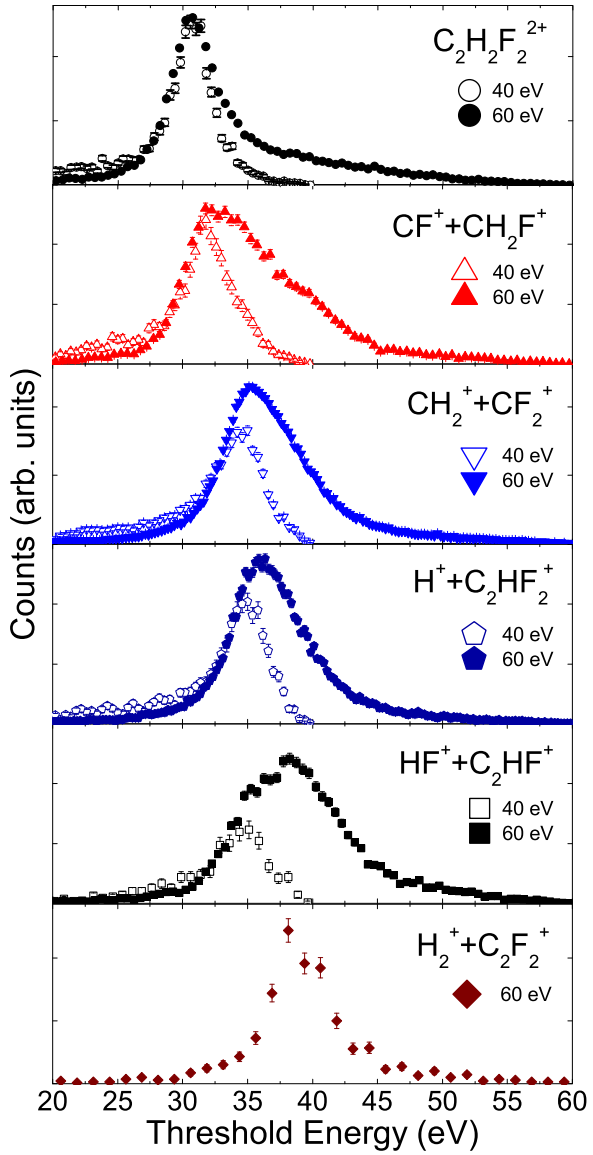

FIG. 3. (Color online) Photo-double-ionization yield as a function of threshold energy (defined as E_{sum} subtracted from the photon energy E_γ) of the different channels of 1,1-$C_2H_2F_2$ using 40- (open symbols) and 60- eV (solid symbols) photons. The error bars indicate the statistical uncertainty in the data. The 40-eV spectra are scaled to match the 60-eV spectra at the threshold energy where the first one peaks. For branching ratio of the channels, see Table I.

The sum of the branching ratios of the DI channels requiring a central C=C bond cleavage is about 63% for all the photon energies used in this study, as shown in Fig. 2(b), while the yield of all the remaining two ionic fragment channels is about 25%, and the rest are $C_2H_2F_2^{2+}$ metastable dications. Note that these relative yields may be different if all other double-ionization channels are included, i.e., two fragment channels with one fragment being neutral and the other being a doubly charged ion, and three-body breakup channels with one fragment being neutral and two fragments being ions, etc.

Some of the latter breakup channels can be identified in the PIPICO spectrum (Fig. 1) in addition to the two-body breakup channels. There are some other stripes visible (not as sharp as the two ionic fragment channels) resulting from the DI into three or more nuclear fragments with at least two of them being charged particles and the other(s) being either charged or neutral. We do not discuss these latter channels in detail in this work as the detection capabilities for neutral fragments in our measurements are lacking. However, we want to point out that the rate of three-body (or more) breakup events in the PDI of 1,1-$C_2H_2F_2$ doubles that of C_2H_4 at 40 eV. We made this comparison using the yields of three-body fragmentation producing two protons and one undetected fragment (marked in the lower half of Fig. 1). In the PDI of 1,1-$C_2H_2F_2$, this three-body yield increases by a factor of 3 as the photon energy is increased from 40 to 70 eV. The contribution from the PDI of residual H_2 in the vacuum chamber would appear as a sharp line in the PIPICO spectrum and is hereby negligible. The dominant three- (or many-) body structure is labeled in Fig. 1 by possible channels $CH_2^+ + CF^+ + F$, $CH^+ + CHF^+ + F$, and $C^+ + CH_2F^+ + F$. We have estimated the yield of the dominant many-body and the two-body channels by integrating the areas within the corresponding stripes in the PIPICO spectrum in Fig. 1. The dominant many-body channel yield is about the same as the sum of the yields of all the individual two-body channels or, specifically, this many-body channel yield is about 10 times higher than the deprotonation channel ($H^+ + C_2HF_2^+$) yield. However, the uncertainty in this ascertainment is large because of the background counts underneath these stripes. The background counts are difficult to eliminate in a two-particle correlation diagram only, especially for the many-body fragmentation case, as our experimental conditions were not set up for separating these channels.

B. Threshold energy

We present the double-ionization threshold energies, evaluated as E_{sum} of the NDI and DI channels subtracted from E_γ, for photon energies of 40 and 60 eV in Fig. 3. For both photon energies, we find that the NDI channel leading to a metastable dication results from the lowest-lying electronic state (likely the electronic ground state of $C_2H_2F_2^{2+}$) with a double-ionization potential of about 31 eV, which is very similar to the PDI of C_2H_4 and C_2H_2 comprising a threshold energy of 30.3 and 33.2 eV, respectively [11]. In all PDI channels of 1,1-$C_2H_2F_2$, larger photon energy leads to a long tail in threshold energy distributions, a result of higher-lying states being accessible at higher photon energy. The first DI channel to open is the $CF^+ + CH_2F^+$ at about 31.5-eV threshold energy. For 60-eV photon energy, the shoulderlike distribution suggests that at least three different states contribute to this dissociation pathway. This fluorine-migration channel seemingly requires less energy than the prompt C=C double-bond breaking which follows next and peaks at around 35 eV, i.e., at almost the same value as the C=C bond cleavage in the PDI of C_2H_4 [11]. In the PDI of C_2H_4, however, the double-bond breaking goes along with the molecular hydrogen elimination channel ($H_2^+ + C_2H_2^+$) and both are preceded by the deprotonation channel ($H^+ + C_2H_3^+$), while in the PDI of C_2H_2 the symmetric breakup ($CH^+ + CH^+$) peaks at 39 eV and is preceded by the deprotonation ($H^+ + C_2H^+$) starting at 34.75 eV and the asymmetric breakup ($C^+ + CH_2^+$) at 35.25 eV [11]. In the PDI of 1,1-$C_2H_2F_2$ at 40-eV photon energy the prompt C=C

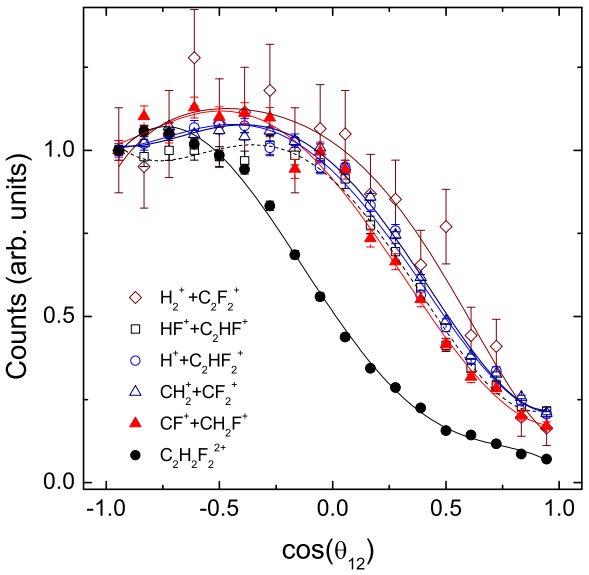

FIG. 4. (Color online) Yield as a function of cosine of the angle θ_{12} between the momenta of the expelled electrons associated with NDI and different DI channels measured for the PDI of 1,1-$C_2H_2F_2$ at 60-eV photon energy. The lines (whose colors match the symbols' color of the corresponding channels) are just to guide the eye.

breaking marks the beginning of a sequence in the threshold energy range of 33.5 to 35 eV comprised of $CH_2^+ + CF_2^+$, $H^+ + C_2HF_2^+$, and $HF^+ + C_2HF^+$. Among these channels, the $HF^+ + C_2HF^+$ channel, which likely demands a fluorine and a hydrogen atom to move simultaneously closer to each other, requires the highest photon energy. For a photon energy of 60 eV it shows a series of three sequences at threshold energies of around 35, 37, and 38 eV, again likely stemming from the population of different electronic states. At the threshold energy of 38 eV, the electronic state responsible for the molecular hydrogen elimination $H_2^+ + C_2F_2^+$ channel can be accessed (not detectable at 40 eV but visible at photon energies of 50, 60, and 70 eV). We explain the possible pathways of this channel in Sec. III E in terms of bond rearrangement and proton migration while comparing to the PDI of C_2H_4.

C. Relative emission angle of electrons

The relative electron angular distribution is shown in Fig. 4 as a function of the cosine of the angle θ_{12} between the momenta of the two electrons emitted by 60-eV photons. There is clearly a difference between the angular distributions of the NDI and DI channels. The electron-electron angular distribution of the NDI is narrow compared to the rest of the DI channels and peaks at around $\cos\theta_{12} = -0.8$ (i.e., θ_{12} around 144°). The relative angle of the two electrons in the NDI channel is guided by the electron-electron repulsion and it is decreasing with increasing sum of the kinetic energy of the electrons ($E_{\rm sum}$), as discussed later in Sec. III D. This is due to the repulsion between two identical charged particles, a phenomenon observed in the PDI of atomic targets [24] and diatomic molecules [25] where photoelectrons with small sum of their kinetic energy $E_{\rm sum}$ repel each other more strongly, and thus emerge into opposite hemispheres. Among the DI channels the relative electron angular distributions follow a trend of increasing width with increasing threshold energy. This effect might be due to the interference of the electronic two-body wave function originating from two different regions of the charge density, which is strongly determined by the extent of the radial wave function of the target orbital as suggested in Ref. [26]. The relative electron angular distributions of the $CH_2^+ + CF_2^+$ and $H^+ + C_2HF_2^+$ channels are similar as their threshold energies are also very similar. This likely means that the dissociation starts from the same potential energy surface leading to the $CH_2^+ + CF_2^+$ breakup along the C-C coordinate or resulting in the deprotonation $H^+ + C_2HF_2^+$ channel along the C-H coordinate. However, the differences in the DI channels are rather subtle and hence require further investigation.

D. Nondissociative ionization

The nondissociative ionization of 1,1-$C_2H_2F_2$ results in a metastable dication ($C_2H_2F_2^{2+}$) (with a lifetime greater than the flight time to the detector, i.e., about 3.6 μs) and two expelled electrons. Note that bound molecular states have a potential well with a dissociation limit higher than the wells' minimum while the metastable or quasibound states have a local minimum, i.e., the dissociation limit is lower than the minimum of the potential well. The dications are clearly separated from other fragment ions in their TOF and position on the detector (not shown here; see Ref. [11] C_2H_4 as an example). The fragment ions CHF^+, if any, would have the same TOF as the metastable dications ($C_2H_2F_2^{2+}$), but compared to the narrow distribution of the dications, they would exhibit a broader TOF peak and a position spread on the detector due to their breakup energy. However, we have not observed any noticeable level of this symmetric breakup ($CHF^+ + CHF^+$) channel. The yield of the NDI channel is obtained by integrating the corresponding electrons' $E_{\rm sum}$ distribution. By surveying the branching ratio as a function of the photon energy in Fig. 2(c), and Table I, it is evident that the NDI yield decreases for higher photon energies. The reason for such a trend is the increasing population of excited states of $(C_2H_2F_2^{2+})^*$ dications at higher photon energies that dissociate, and hence result in the increased yield of the DI channels. The measured yield of the NDI channel at 40-eV photon energy is about 15% (see Table I) and is more than double the corresponding NDI yield (about 6%) of C_2H_4 at a similar photon energy [11]. This can be attributed to a stronger binding in 1,1-$C_2H_2F_2$ due to the presence of F atoms.

The energy correlation map between the two photoelectrons measured for 40-eV photons in coincidence with the dications is shown in Fig. 5(a) as a density plot of the yield as a function of kinetic energy of the first and the second electron (E_1, E_2) (note that the numbering of the electrons is arbitrary). One can readily see an almost constant density of counts along a diagonal feature at about 9.4 eV. As in the case of the PDI of C_2H_4 [11], the structureless energy sharing can be assigned to a direct ionization process, which emits two electrons from the outermost orbital of the neutral molecule simultaneously (sometimes also referred to as TS1 electron-electron knockout process). From the electrons' sum kinetic energy of 9.4 eV we deduce a threshold energy of 30.6 eV (2.8-eV full width at

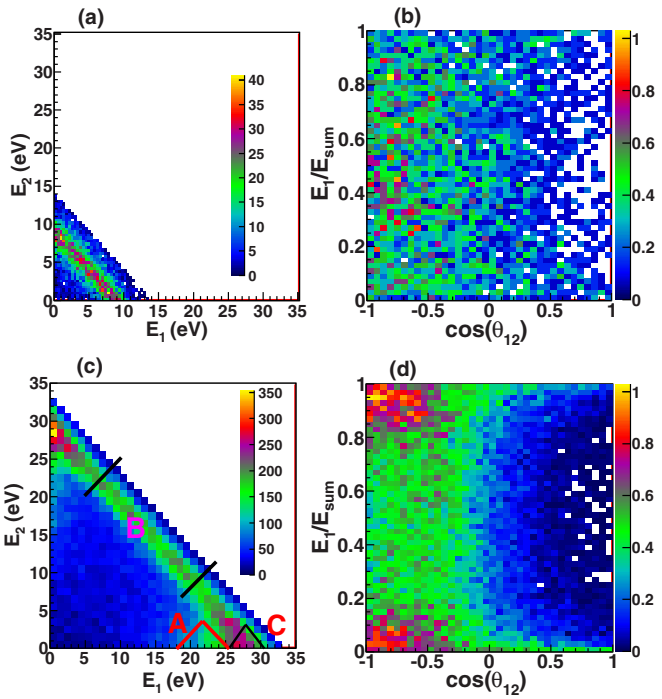

FIG. 5. (Color online) (a) Density plot of the kinetic energies of the two electrons measured in coincidence with the dications ($C_2H_2F_2^{2+}$). (b) Yield as a function of the cosine of the relative angle θ_{12} between the two electrons' momenta and the energy sharing. Both (a) and (b) were measured using a photon energy of 40 eV. (c), (d) Same as (a) and (b), but for 60-eV photon energy. The regions A, B, and C in panel (c) are used later on to identify the different ionization processes.

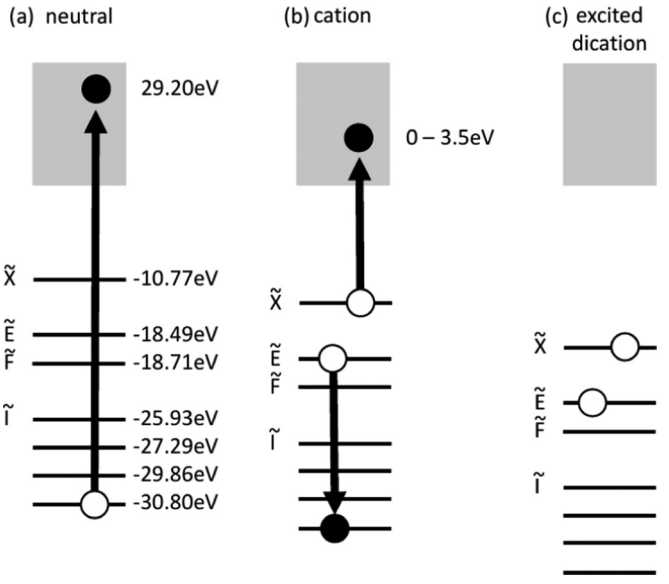

FIG. 6. Schematic drawing of the Auger decay following the PDI of 1,1-$C_2H_2F_2$ at a photon energy of 60 eV. (a) Photoionization of the lowest-lying $\widetilde{I}$ state of the neutral molecule (adapted from [29]). (b) Recombination of the vacancy and emission of the Auger electron in the cation. (c) Resulting excited dication. Note that the $\widetilde{I}$ state represents a band of lines with different intensities that have different single IPs. The lines corresponding to different ionic states in (b) and (c) are shifted down (by an unknown value) compared to that of the neutral molecule in (a) due to the change of the effective potential after the ionization of the first electron.

half maximum) for the NDI channel, which is slightly higher than the previously reported double-ionization potential of 1,1-$C_2H_2F_2$ (28.5 eV in Ref. [27] or 29.3 eV using the difference energy of 19 eV between the singly and doubly charged molecular ions in Ref. [15] and the first ionization potential of 10.3 eV from Ref. [28]). We do not have a clear explanation for this small energy difference of a few eV. The broad distribution in our experiment indicates that both the electronic ground state of the dication with a nonplanar geometry and the excited state with a planar geometry, contribute to the NDI channel (these two states are only 0.25 eV apart [15] and are not resolved in our measurements).

The electron energy correlation map for 60-eV photons, which is shown in Fig. 5(c), is at first glance similar in structure to the lower photon energy case [Fig. 5(a)]. The diagonal feature at around 29 eV is a result of the direct ionization process. However, one can also note that the density is higher when one of the electrons carries almost all of the available excess energy. What appear to be small islands at the end of the diagonal in Fig. 5(c) are actually the result of an overlap of other (lower-lying) diagonal broken lines with the direct ionization channel. This hints towards an indirect double-ionization process. Energetically, these islands [like the one marked as A in Fig. 5(c)] can be assigned to a molecular Auger decay (see Fig. 6). In this scenario, the lowest $\widetilde{I}$ neutral state (single IP of −30.8 eV) and the satellite states (single IP of −30 to −32.6 eV, not shown here) taken from Refs. [29,30] are photoionized such that the resulting photoelectrons have energies of 29 to 27.4 eV for a photon energy of 60 eV. The vacancy in the remaining cation can then be filled by a transition of an electron from the higher lying $\widetilde{E}$ or the $\widetilde{F}$ cation states subsequently emitting an Auger electron from the $\widetilde{X}$ state of the cation with a kinetic energy of 0 to 3.5 eV. This leaves an excited but metastable dication behind, which diminishes the amount of available excess energy in comparison to the production of the ground-state dications in the direct ionization process, and thus results in a shift towards lower E_{sum} energies. Lower-energy photoelectrons obviously correspond to the ionization of the satellite states. It is not clear why only states and orbitals below a single IP of −30 eV of the neutral molecule are involved in this molecular Auger decay though.

The feature of two overlapping processes is more distinct in Fig. 5(d) where we plot the two-electron yield as a function of the electron energy sharing (E_1/E_{sum}) and the cosine of the relative angle (θ_{12}) between the two electrons' momenta. The electron energy sharing is flat for 40 eV [see Fig. 5(b)], and thus dominated by the direct double-ionization process. It suddenly shows a U-shape-like structure at a photon energy of 50 eV (not shown), which does not significantly change at 60 eV [shown in Fig. 5(d)] and 70 eV (not shown here). The reason for this sharp onset is yet unknown; it likely stems from the fact that the direct double-ionization cross section vanishes rather quickly with increasing photon energy. For a photon energy of 40 eV, there are no obvious structures in the relative electron angle [see Fig. 5(b)], while at 60 eV one can see an enhanced back-to-back emission for energy-sharing

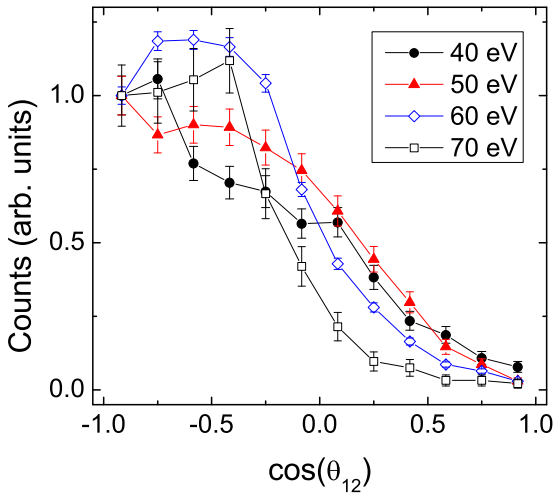

FIG. 7. (Color online) Yield as a function of cosine of the angle θ_{12} between the momenta of two emitted electrons, with equal energy sharing, measured in coincidence with the dications ($C_2H_2F_2^{2+}$) from the nondissociative ionization of 1,1-$C_2H_2F_2$ for different photon energies (40–70 eV).

values approaching 0 and 1 in Fig. 5(d). This means that both electrons are preferably emitted to opposite directions when one of the two electrons carries most of the energy. One can see that the indirect ionization is enhanced even though the overall yield of the metastable dications decreases for higher photon energies [see Fig. 2(c)].

The yield of the NDI channel as a function of the cosine of the angle θ_{12} for equal energy sharing ($E_1/E_{\rm sum} \sim 0.5 \pm 0.1$) are shown in Fig. 7 for all measured photon energies. The distribution is wide and peaks around $\cos\theta_{12}$ of -1.0 (i.e., $\theta_{12} = 180^\circ$) for a photon energy of 40 eV. With increasing photon energy, the width of the angular distribution decreases. Moreover, the peak position of the distribution also changes towards $\cos\theta_{12}$ of -0.5 (i.e., $\theta_{12} = 120^\circ$). As mentioned in Sec. III C, this is due to the repulsion between the two electrons, a phenomenon observed in the PDI of atomic and diatomic targets [24,25].

We can verify that indirect double-ionization (molecular Auger) and direct double-ionization (TS1) processes lead to the formation of metastable dications in the PDI of 1,1-$C_2H_2F_2$ by studying the angular distribution of the electrons in more detail. For this we select different regions of the electron energy-sharing distribution marked as A and B in Fig. 5(c). The angular distributions are shown in Fig. 8 [top row, (a)–(c)] as a polar angle (θ) of the electron momentum with respect to the light polarization and the bottom row [(d)–(f)] as a relative angle (θ_{12}) between the momenta of the two electrons.

The angular distribution (θ) of the Auger electrons (i.e., low kinetic energy electrons), from region A marked in the energy sharing in Fig. 5(c), is shown in Fig. 8(a). The angular distribution can be parametrized according to

$$I(\theta) = \frac{\sigma}{4\pi}\left[1 + \frac{\beta}{2}(3\cos^2\theta - 1)\right],$$

where β is the asymmetry parameter and σ is the total photoionization cross section [31–34]. For the Auger electron angular distribution, β is found to be around zero (about 0.02 ± 0.03) indicating an isotropic distribution. The angular distribution of the corresponding photoelectrons (high kinetic energy electrons), shown in Fig. 8(b), from the same region A is very different and has a β parameter of about 1.39 ± 0.13, i.e., closer to the value of 2 which characterizes the emission of a dipole distribution parallel to the polarization vector of light.

The relative angle (θ_{12}) between the momenta of two electrons [as a pair from region A in Fig. 5(c)] is presented in Fig. 8(d). This resembles a near-isotropic distribution of the second electron indicating that its emission direction is independent of the direction of the photoelectron (the photoelectron direction is chosen to be always to the right in the figure, as indicated by the arrow). Such an isotropic distribution is expected for a molecular Auger process, which we assume takes place as discussed above.

The β parameter of the photoelectrons from the direct double ionization [i.e., region B in Fig. 5(c)] is about -0.02 ± 0.02, as shown in Fig. 8(c), indicating an isotropic angular distribution. The relative angular distribution of electrons from the direct double ionization (TS1 process) is shown in Fig. 8(e). Moreover, the relative angle between the electrons from direct ionization with equal energy sharing ($E_1/E_{\rm sum} \sim 0.5 \pm 0.1$) is presented in Fig. 8(f). Both distributions show a preferred emission into opposite hemispheres. We note a slightly suppressed back-to-back emission for the case of equal electron energy sharing in the direct ionization [Fig. 8(f)]. This is due to a selection rule valid for dipole transitions based on parity conservation, and is well known in the PDI of atomic and diatomic systems with linear polarized light [3]. Already in the PDI of H_2 (D_2), this selection rule is somehow relaxed as the molecular axis breaks the spherical symmetry of the corresponding two-electron He case [3], and thus the nodal line of the atomic case collapses to a nodal point, which results in a less sharp zero in the relative angles of 180° between the two electrons of H_2 molecule. Hence, it is not surprising that we observe counts near a back-to-back emission scenario in the double ionization of 1,1-$C_2H_2F_2$.

As presented above, the relative angle between the two electrons for the indirect process is isotropic [Fig. 8(d)], while for the direct process the emission is preferentially back-to-back [Fig. 8(e)]. We note that for the electrons at the corner of the main diagonal between 25 and 31 eV energy [region C in Fig. 5(c)], the relative angle between the momenta of two electrons features a mix of indirect and direct processes. The distribution is shown in Fig. 8(g) and it is dominated by the direct process resulting in more emissions into the opposite hemispheres compared to the emission of electrons in the same direction.

E. Dissociative ionization

Before we discuss each DI channel in detail, we present an overview of the four most prominent fragmentation channels for photon energies of 40, 50, and 60 eV (70-eV data sets are omitted here due to low statistics). As in NDI, the electron-electron energy correlation spectra of all major DI channels, shown in Fig. 9, exhibit two features: (a) a diagonal line showing a continuous distribution of counts,

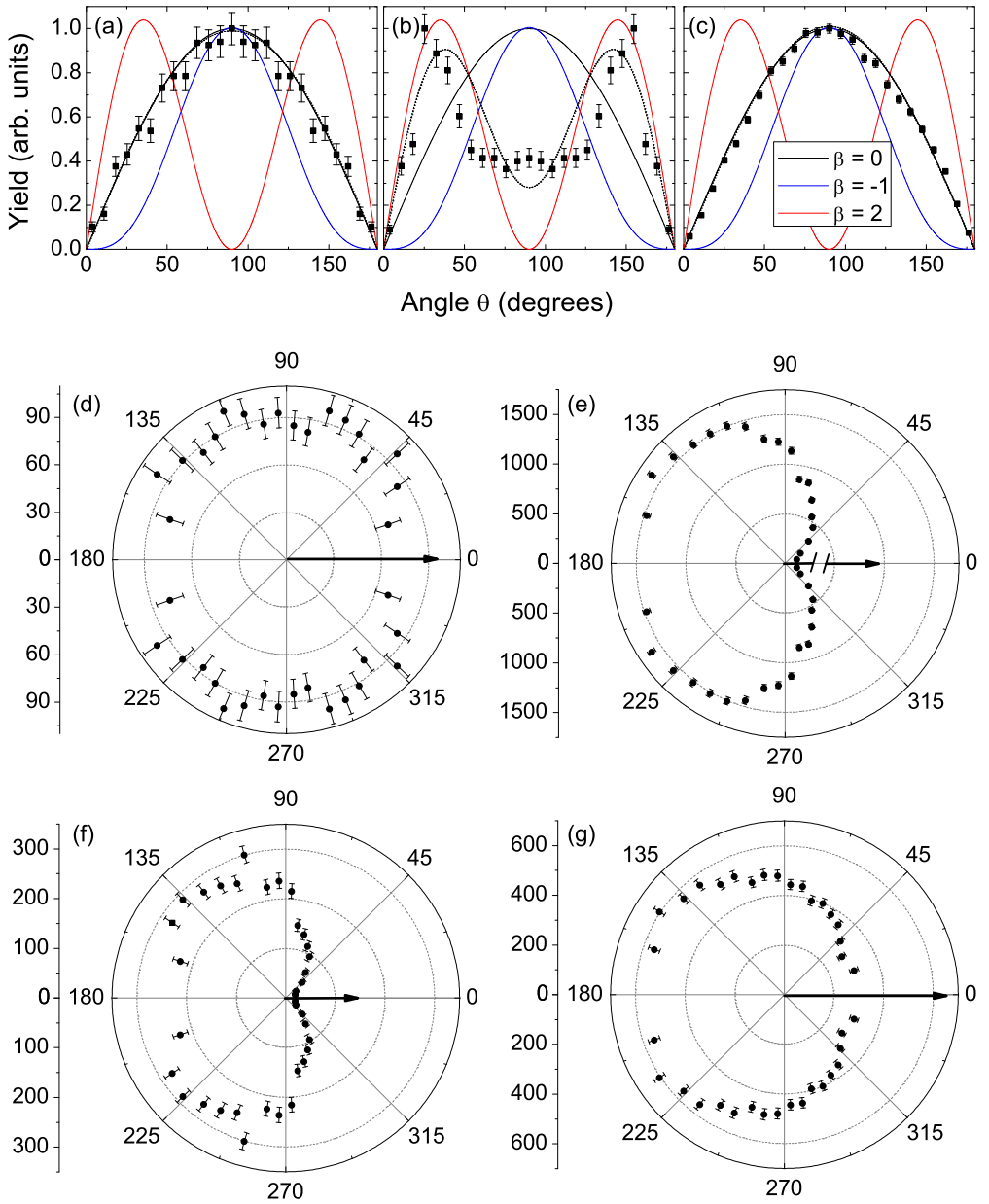

FIG. 8. (Color online) Top row: Polar angle (θ) of electrons, with respect to the polarization of light, measured in coincidence with the dications ($C_2H_2F_2^{2+}$) from the nondissociative ionization of 1,1-$C_2H_2F_2$ using 60-eV photon energy for (a) Auger electron (i.e., the electrons with low kinetic energy), (b) photoelectron (i.e., the electrons with high kinetic energy) both from region A in Fig. 5(c), and (c) photoelectrons from region B in Fig. 5(c) (i.e., both of the electrons have similar range of kinetic energy). Bottom rows: Plot of the cosine of the relative angle (θ_{12}) between the momenta of two electrons for (d) indirect double ionization [i.e., molecular Auger decay region A marked in the energy correlation map in Fig. 5(c), i.e., islands between 18 and 25 eV], (e) direct double ionization [region B along the major diagonal in the Fig. 5(c)], (f) direct double ionization with equal energy sharing [i.e. a narrow region in the middle of the diagonal in Fig. 5(c)], and (g) mix of indirect and direct double ionization with asymmetric energy sharing between electrons [islands between 25 and 31 eV from region C in Fig. 5(c)]. The first electron always goes to the right as indicated with the arrow. The lengths of the arrows correspond to a very asymmetric electron energy sharing in panels (d) and (g), and a rather equal energy sharing in the (e) and (f) panels.

which stems from the direct ionization process, and (b) islands at the end of the diagonals suggesting an indirect ionization process, i.e., a sequential process. At 40-eV photon energy the contribution from indirect double ionization is rather low for the NDI [see Fig. 5(a)] and all DI channels (i.e., the top row in Fig. 9); in this way, they are comparable to the PDI of C_2H_4 [11]. However, at 50-eV photon energy, i.e. about 20 eV above the double-ionization threshold (middle row in Fig. 9) this additional indirect fragmentation pathway opens up and results in an increasingly asymmetric electron energy sharing with increasing photon energy (see for instance bottom row in Fig. 9, i.e., the 60-eV photon energy case). As in the NDI case, this characteristic can be attributed to a two-step ionization decay process. In the case that this process happens very fast, this can be related to a molecular Auger decay, i.e., an immediate transition in the parent molecular

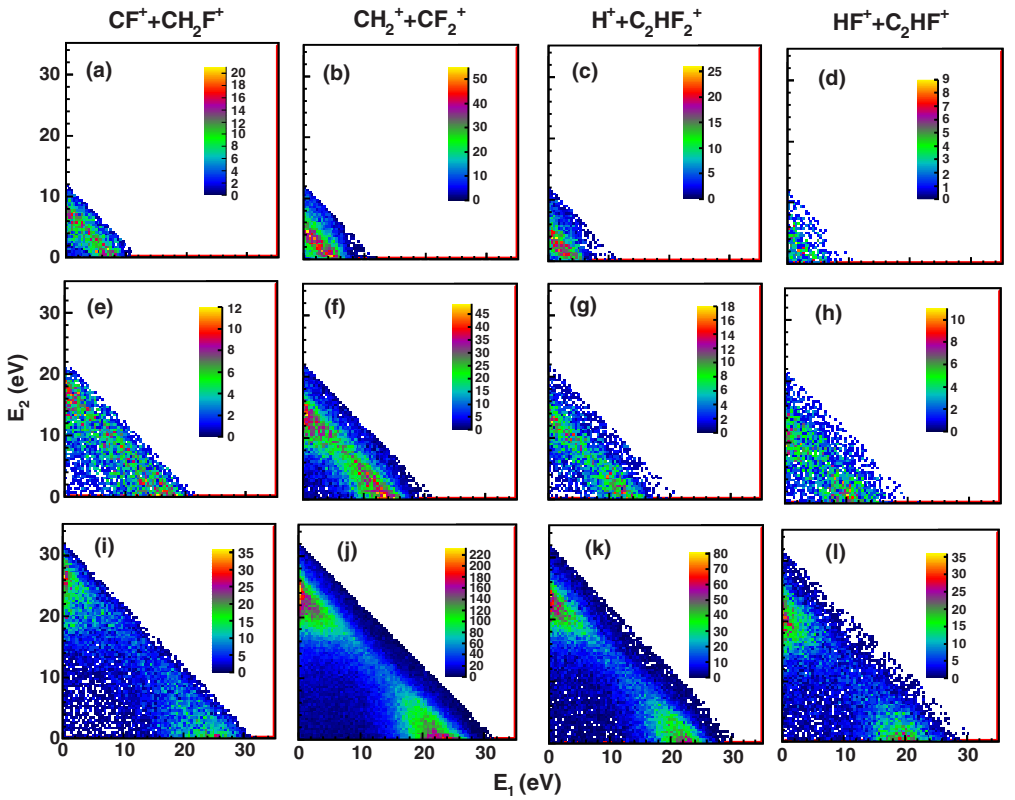

FIG. 9. (Color online) Electron energy correlation maps, shown as density plots as a function of kinetic energy of two emitted electrons (E_1, E_2) for DI channels using 40-, 50-, and 60-eV photon energies, from top to bottom row, respectively: first column $CF^+ + CH_2F^+$, second column $CH_2^+ + CF_2^+$, third column $H^+ + C_2HF_2^+$, and fourth column $HF^+ + C_2HF^+$ channels.

cation upon photoabsorption. However, with increasing photon energy, the molecule can be ionized and electronically excited simultaneously. The excited cation can dissociate subsequently and undergo autoionization while it relaxes to a lower-lying dication state at large internuclear distances expelling a second electron. While the electron energy sharing is similar in both scenarios, the autoionization is slower than the Auger process, and thus provides time for nuclear motion to take place (e.g., stretching or conformation changes) that may be reflected in the KER distribution.

The electron energy sharing as a function of KER is shown in Fig. 10 for the four major DI channels. For 40-eV photon energy, the electron energy sharing distribution is uniform with the KER. However, this changes for higher photon energies where the electron energy sharing becomes more asymmetric. For an unequal electron energy sharing at photon energies of 50 and 60 eV, we notice a broader KER distribution than for the 40-eV energy case (see Fig. 10). While the higher KER can result from excited electronic states with different slopes that would explain the shoulderlike feature, the lower KER either stems from shallow excited PESs or indicates that the molecule had time to stretch, which would point towards an autoionization process. This behavior is most prominent for the $CH_2^+ + CF_2^+$ channel and the deprotonation $H^+ + C_2HF_2^+$ as well the $HF^+ + C_2HF^+$ breakup (second, third, and fourth columns in Fig. 10) at 60 eV (bottom row of Fig. 10). The electron energy sharing for final states with a KER of 4.5 eV ($CH_2^+ + CF_2^+$) and a tail around a KER of 6.5 eV ($H^+ + C_2HF_2^+$) became exclusively asymmetric. In order to completely discern between the two indirect ionization processes (i.e., molecular Auger and autoionization) in the DI channels molecular frame photo (and Auger and autoionization) electron angular distributions (MFPADs and MFAADs) as a function of KER need to be measured. This is beyond the scope of this paper and it will be addressed in future experiments.

We now discuss the DI channels of the PDI of 1,1-$C_2H_2F_2$, which result in two ionic fragments in more detail. The channels are listed in the following in the order of increasing threshold energy (see Sec. III B).

1. $CF^+ + CH_2F^+$

The electron-ion energy map for the $CF^+ + CH_2F^+$ channel, i.e., the PDI yield as a function of KER and E_{sum}, is shown in Fig. 11(a). While the hydrogen atoms remain bound to their respective carbon atoms, this channel clearly results from the migration of one of the F atoms followed by the central C=C bond breaking, a process that does not happen instantly but likely takes several tens of femtoseconds. The fragment ions CF^+ and CH_2F^+ are very close in their mass and experimentally represent a challenge to distinguish from the symmetric ($CHF^+ + CHF^+$) channel in the PIPICO spectrum shown in Fig. 1. However, our full 3D momentum analysis requiring momentum and energy conservation enables us to isolate this channel and show that the symmetric channel yield is very low, on the order of the impurity level of the 1,1-$C_2H_2F_2$ gas bottle (below 1%). We believe that no symmetric breakup is

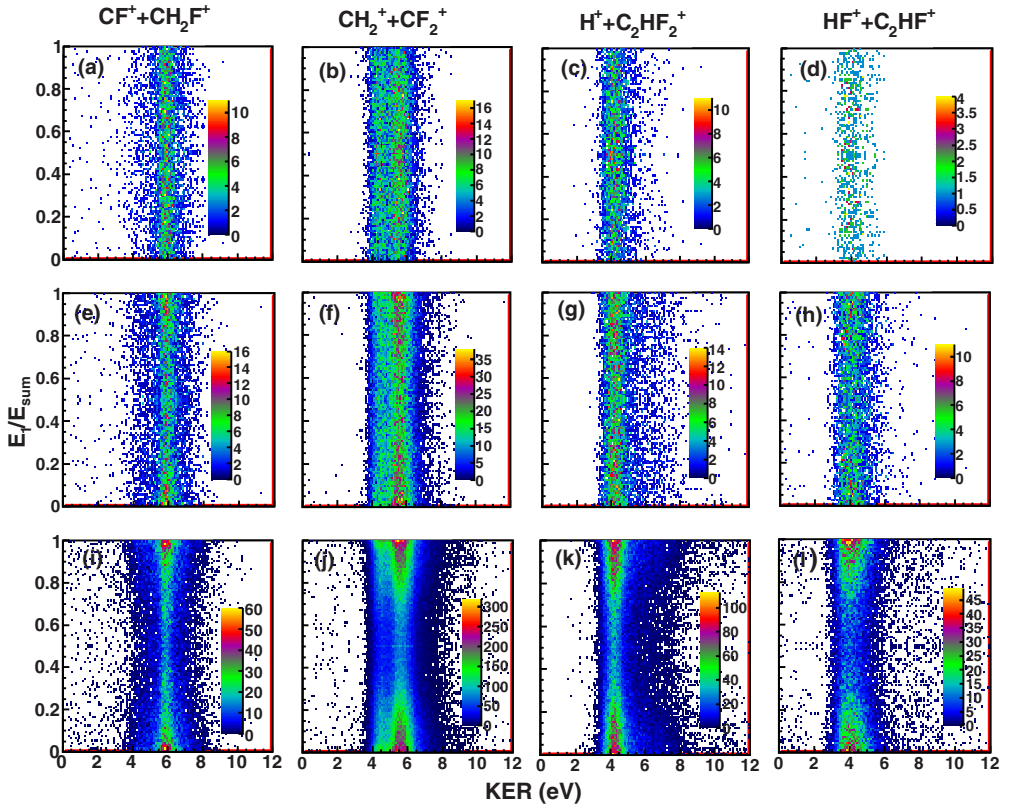

FIG. 10. (Color online) Yield as a function of KER and energy sharing ($E_1/E_{\rm sum}$) for the major DI channels using 40-, 50-, and 60-eV photon energies, from top to bottom row, respectively: first column $CF^+ + CH_2F^+$, second column $CH_2^+ + CF_2^+$, third column $H^+ + C_2HF_2^+$, and fourth column $HF^+ + C_2HF^+$ channels.

produced by the PDI of 1,1-$C_2H_2F_2$ but that the traces of CHF^+ ions originate from the PDI of residual 1,2-cis/trans-$C_2H_2F_2$ of our gas bottle.

The KER distribution of the $CF^+ + CH_2F^+$ channel, shown in Fig. 11(a), has one major feature peaked around 6 eV. This corresponds to a higher $E_{\rm sum}$, which in turn indicates that a

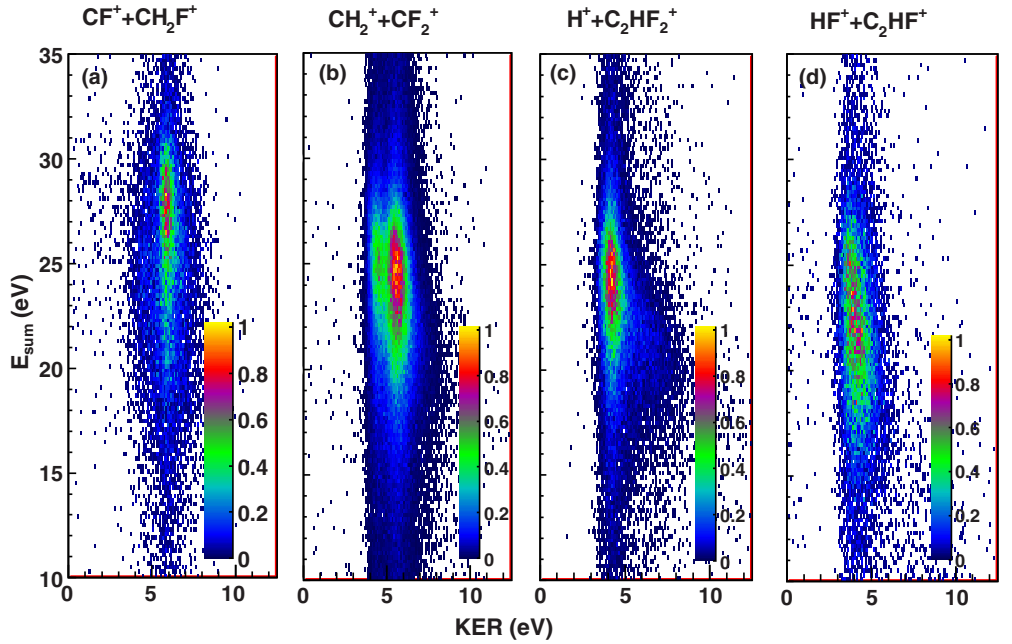

FIG. 11. (Color online) Electron-ion energy maps of the PDI of 1,1-$C_2H_2F_2$ shown as a density plot as a function of KER and $E_{\rm sum}$ for DI channels using 60-eV photon energy: (a) $CF^+ + CH_2F^+$, (b) $CH_2^+ + CF_2^+$, (c) $H^+ + C_2HF_2^+$, and (d) $HF^+ + C_2HF^+$.

lower-lying state is responsible for the pathway leading to this feature. We also note that this KER distribution drops much more gradually toward lower KER values than the KER distribution of the other channels shown in Figs. 11(b)–11(d) which comprise a sharp cutoff at lower values.

2. $CH_2^+ + CF_2^+$

The prompt breaking of the central C=C bond of the 1,1-$C_2H_2F_2$ dication produces the two fragment ions CH_2^+ and CF_2^+. The overall relative yield of the $CH_2^+ + CF_2^+$ channel is the highest for all the photon energies used in our measurements and shows a maximum at 60-eV photon energy [see Fig. 2(a)]. The electron-ion energy map for the $CH_2^+ + CF_2^+$ channel is shown in Fig. 11(b). The KER distribution has two prominent features and these two peaks (one at 4.5 eV and the other at 5.5 eV) are separated by about 1 eV. The E_{sum} distributions corresponding to these two different KER features are also peaked 1 eV apart. This indicates that this fragmentation pathway comprises at least two electronic states which vary by 1 eV in their threshold energies and also have about the same energy difference in their asymptotic limits.

In addition to the two features discussed above, we see a small tail extending towards higher KER and lower E_{sum}, which shows some photon energy dependence (see Fig. 10, second column: elusive at 40-eV but visible at 50-eV and pronounced at 60-eV photon energies). The rather extensive change in E_{sum} of about 2 eV [see Fig. 11(b)] suggests that another electronically excited state is populated. It appears that this different intermediate dication state has a lower dissociation limit which is necessary to explain the corresponding increase in KER.

The events with low KER (4.5 eV) resemble the minor feature and the peak with 5.5 eV is similar to the main feature in the symmetric breakup channel observed in the PDI of C_2H_4 using 40.5-eV photons [11]. The relative yield of this low-KER feature is enhanced for all photon energies used in the 1,1-$C_2H_2F_2$ study compared to the corresponding yield in the minor feature of the symmetric breakup in C_2H_4. The fragmentation pathway of the minor feature in the symmetric breakup channel of ethylene involves the electronic ground state (S_1) and the first-excited singlet state (S_2) [11]. The initial ionization step populates the S_2 state and subsequently this population is transferred to the S_1 state via a conical intersection leading to the breaking of the central C=C bond. It is plausible to assume a similar pathway for the low-KER feature in the 1,1-$C_2H_2F_2$ breakup, but we lack theoretical and experimental information about the electronic states of the 1,1-$C_2H_2F_2$ dication, which could support this scenario.

3. $H^+ + C_2HF_2^+$

The DI channel in which one proton is lost after the PDI of 1,1-$C_2H_2F_2$, namely $H^+ + C_2HF_2^+$, is often called deprotonation. In this breakup channel, a hydrogen migration may or may not be involved; our experimental technique can not unambiguously distinguish between these two pathways. The branching ratio of this breakup channel, shown in Fig. 2(a), is rather constant (around 16%) over the four photon energies used in our measurements. The KER distribution shown in Figs. 10(k) and 11(c) is broad. It peaks around 4.5 eV and has a long tail extending to high KER. As mentioned in the discussion of the previous breakup channel ($CH_2^+ + CF_2^+$), this long KER tail points towards the population of a higher-lying electronic state with a lower dissociation limit. The E_{sum} distribution peaks at around 23 eV for a photon energy of 60 eV. This results in a vertical energy of 37 eV, which in turn indicates that excited states $(C_2H_2F_2^{2+})^*$ are involved in this fragmentation channel. This assumption is supported by the tail towards higher KER and smaller E_{sum} in Fig. 11(c), which is more pronounced than the similar feature in the $CH_2^+ + CF_2^+$ breakup channel discussed above. As can be expected, this is also a function of photon energy (see Fig. 10, third column: elusive at 40-eV photon energy but becomes distinct at 50 eV and most prominent at 60 eV).

4. $HF^+ + C_2HF^+$

The KER and E_{sum} distributions of the $HF^+ + C_2HF^+$ channel [Fig. 11(d)] are broad and the electron energy sharing [Fig. 10(l)] is very asymmetric. This supports an autoionization scenario and suggests more than one fragmentation pathway in this breakup channel that we can not resolve in our measurement. However, the threshold energy shown in Fig. 3 displays at least two peaks for this $HF^+ + C_2HF^+$ channel: one at around 35 eV and the other one around 38 eV. In order to produce an HF^+ fragment, a conformation change must have happened. However, there are at least three possibilities for this to proceed: (a) the hydrogen atom migrated to one side, (b) the fluorine atom moved to the opposite end, or (c) both constituents migrated towards each other along the C=C bond. We see that the yield of this channel increases with the photon energy while the $CF^+ + CH_2F^+$ channel depletes [see Fig. 2(a)]. The threshold energy for these two fragmentation pathways is ~32 eV for the $CF^+ + CH_2F^+$ channel and ~39 eV for the $HF^+ + C_2HF^+$ channel (see Fig. 3). This hints towards the population of higher-lying electronic states being accessed with increasing photon energy, and those states dissociate to HF^+ and C_2HF^+ final products. The opposite trends in the yield compared to the $CF^+ + CH_2F^+$ channel and the population of a higher-lying state point towards the simultaneous migration of the H and F atoms approaching each other and forming a bond before being expelled as an HF^+ ion [scenario (c) from above].

5. $H_2^+ + C_2F_2^+$

The yield of the molecular hydrogen-ion elimination $H_2^+ + C_2F_2^+$ channel as presented in Fig. 2(a) and Table I is surprisingly very low (less than 1%) for all photon energies used in our investigation. The electron-ion energy map for a photon energy of 60 eV is shown in Fig. 12(c). This map comprises one feature only, though, the statistics is very low. The KER distribution has a peak around 4 eV and the corresponding E_{sum} distribution peaks at about 21.7 eV, suggesting that the responsible state for this channel is a highly excited state with a threshold energy of 38.3 eV.

In order to form a molecular hydrogen ion (H_2^+), one could assume that the C-H bonds between the hydrogen atoms and the C atom stretch in a scissoring mode and two hydrogen atoms approach each other to form a bond, i.e., the C=C bond contracts and the C-H_2^+ bond elongates which ultimately

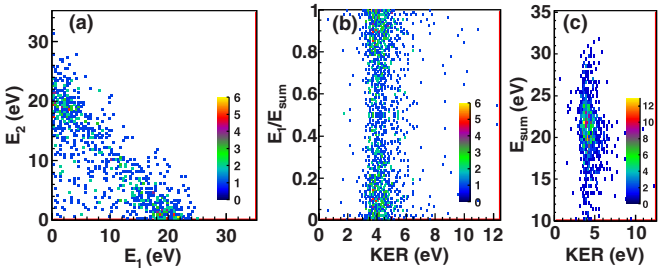

FIG. 12. (Color online) (a) Electron energy correlation map (similar to Fig. 9), (b) PDI yield as a function of KER and electron energy sharing (similar to Fig. 10), and (c) PDI yield as a function of KER and E_{sum} (similar to Fig. 11), all panels for the $H_2^+ + C_2F_2^+$ channel at 60-eV photon energy.

results in the emission of an H_2^+ ion from the parent ion. This argument was used in the PDI of C_2H_4 at a photon energy of 40.5 eV [11], where we found a branching ratio for the molecular hydrogen-ion elimination of the order of 7%. This multistep scenario was supported by the calculated PESs which showed a pathway around the barrier for direct dissociation. While comparing the structure of 1,1-$C_2H_2F_2$ and C_2H_4 one can think that molecular hydrogen-ion elimination is likely to occur in both molecules since two hydrogen atoms are bonded to the same carbon atom in both cases (although there are fluorine atoms bonded to the other carbon atom in case of 1,1-$C_2H_2F_2$). Moreover, the bond angles and internuclear distances are very similar in both species [15]; only the partial charge of the C atom next to the fluorine in 1,1-$C_2H_2F_2$ is higher due to the high electronegativity of the latter atom. However, no obvious argument can be found that would prevent this dissociation scenario from happening in the PDI of 1,1-$C_2H_2F_2$. The low branching ratio of below 1% is thus very surprising. This observation suggests that a molecular hydrogen elimination is perhaps more likely to happen when an intermediate ethylidenelike molecule ($HCCH_3$) can be formed via proton migration as suggested in Refs. [35–39].

Hydrogen migration may play an even bigger role in the molecular hydrogen elimination than one would first suspect. In the case of photodissociation of ethylene, it has been proposed that the removal of H_2 molecules occurs via a transition state in which one of the hydrogen atoms moves across the C=C double bond and forms an ethylidene structure [35–39]. If such a mechanism is needed for the molecular hydrogen elimination, it can not take place in 1,1-$C_2H_2F_2$ or 1,2-cis/trans-$C_2H_2F_2$ since there is no extra hydrogen atom to migrate across the C=C double bond. On the other hand, the observation of the $HF^+ + C_2HF^+$ channel proves that an ethylidene-type structure formation can take place in the PDI of 1,1-$C_2H_2F_2$ where one of the fluorine atoms migrates across the C=C double bond. However, when the intermediate ethylidenelike state decays, it favors the generation of HF fragments rather than H_2 or even F_2 elimination.

Alternatively, one could speculate that a molecular hydrogen-ion elimination is more likely to occur when two protons which are bound to different atoms approach each other and form a bond. This is conceivable for the PDI of C_2H_4. For the PDI of 1,1-$C_2H_2F_2$, we actually found the relative yield of molecular hydrogen-ion elimination to be on the order of impurities by 1,2-cis/trans-$C_2H_2F_2$ molecules. One possibility is that the two hydrogen atoms from two sides of the C=C double bond came together in 1,2-cis/trans-$C_2H_2F_2$ instead of two H atoms from the same carbon atom forming an H_2 on one side of the double bond in 1,1-$C_2H_2F_2$. However, further work is needed to confirm such a mechanism. Ibuki *et al.* in Ref. [14] did not report on the observation of the H_2^+ ion in their measurements with 1,1-$C_2H_2F_2$. In the case of 1,1-$C_2H_2D_2$, the TOF of H_2^+ overlaps with that of D^+ and hence can not be distinguished. However, their [14] observation of D_2^+ yield (below 1%) is on the same order of magnitude as the yield of the $H_2^+ + C_2F_2^+$ channel in our present measurement.

IV. SUMMARY

We have presented the PDI of 1,1-difluoroethylene (1,1-$C_2H_2F_2$) using linearly polarized single photons with energies ranging from 40 to 70 eV. We have observed a large NDI yield for low photon energy, which is decreasing with increasing photon energy (15% at 40 eV to 5% at 70 eV). It is clearly higher than the NDI yield of C_2H_4 (about 6% for 40.5-eV photon energy) and lower than that of C_2H_2 (about 60% for 42-eV photon energy). We attribute this behavior to an omission of a propensity rule that is applicable in centrosymmetric molecules only and larger Franck-Condon factors (see [11]) as well as an increasing population of excited states of the dication leading to the DI channels. In addition, our measurements suggest direct (TS1) and indirect (molecular Auger) ionization processes responsible for the production of metastable dications, while additional contribution from the autoionization in the dissociation is possible only for DI channels. The angle between the two expelled electrons' momenta exhibits the effect of electronic repulsion similar to what is observed in the photo-double-ionization of atomic targets.

Among the DI channels, the $CH_2^+ + CF_2^+$ breakup, which results from the cleavage of the central C=C bond, dominates. We do not observe any significant yield of a symmetric breakup channel leading to two CHF^+ fragments because it requires multiple bond breaking followed by a rearrangement of the constituent atoms and has thus proven to be very unlikely. In some of the DI channels, namely, $HF^+ + C_2HF^+$ and $CF^+ + CH_2F^+$, we have observed intriguing phenomena of bond rearrangement involving the migration of constituent hydrogen and fluorine atoms. For a H_2^+ formation to occur, it may be more favorable that the two H atoms are attached initially to two different C atoms of the double bond: a configuration absent in the 1,1-$C_2H_2F_2$ molecule but present in the cis and trans isomers. The impurities of our target gas with the latter isomers are in the order of 1%, and it thus may be possible that the low yield of molecular hydrogen elimination (1%) observed in our experiments is not due to the PDI of 1,1-$C_2H_2F_2$ at all but stems from the PDI of the isomers.

One intriguing observation is that the same set of states (threshold energy of 30 to 45 eV) are populated in the PDI of 1,1-$C_2H_2F_2$ while using different photon energies over the range of 40 to 70 eV. The results shown in the case of 60-eV photon energy indicate that the states with threshold energy

above 45 eV are not populated and most likely are not involved in the fragmentation pathways at least for the channels with two ionic fragments observed here. One possible explanation for this observation is that such higher-lying states result in channels with three or more atomic or ionic fragments. It will be interesting to find out whether such higher-lying states exist and if so why they are not populated in the PDI of the 1,1-$C_2H_2F_2$ molecule. This may be one of the motivations to carry out intricate calculations of the potential energy surfaces of $C_2H_2F_2^{2+}$ molecular dication. Moreover, the PDI of $C_2H_2F_2$ is an ideal testbed to experimentally and theoretically study the migration of light hydrogen atoms and heavy fluorine atoms in a time-resolved way. Photon energies in the range of 40 to 70 eV are already accessible with sources such as high harmonic generation or soft x-ray free-electron lasers to perform one or two color pump-probe experiments. Clearly, the molecular states of the dication and the intermediate cation states need to be calculated in order to understand the ionization mechanisms, the dissociation dynamics, and electron-electron correlations suggested in this paper.

ACKNOWLEDGMENTS

We thank the staff of the Advanced Light Source, in particular A. Aguilar and D. Kilcoyne from beamline 10.0.1, for their outstanding support. This work was supported by the Director, Office of Science, Office of Basic Energy Sciences, and by the Division of Chemical Sciences, Geosciences, and Biosciences of the US Department of Energy at LBNL under Contract No. DE-AC02-05CH11231. B.B., M.Z., and I.B. acknowledge support from the same funding agency under Grant No. DE-FG02-86ER13491. We acknowledge support from the DAAD and the DFG. Support with the delay-line detectors was provided by ROENTDEK.

[1] T. Ishihara, K. Hino, and J. H. McGuire, Phys. Rev. A **44**, R6980 (1991).
[2] R. Dörner, H. Bräuning, J. M. Feagin, V. Mergel, O. Jagutzki, L. Spielberger, T. Vogt, H. Khemliche, M. H. Prior, J. Ullrich, C. L. Cocke, and H. Schmidt-Böcking, Phys. Rev. A **57**, 1074 (1998).
[3] T. Weber, A. Czasch, O. Jagutzki, A. Müller, V. Mergel, A. Kheifets, J. Feagin, E. Rotenberg, G. Meigs, M. H. Prior, S. Daveau, A. L. Landers, C. L. Cocke, T. Osipov, H. Schmidt-Böcking, and R. Dörner, Phys. Rev. Lett. **92**, 163001 (2004).
[4] T. Weber, A. O. Czasch, O. Jagutzki, A. K. Müller, V. Mergel, A. Kheifets, E. Rotenberg, G. Meigs, M. H. Prior, S. Daveau, A. Landers, C. L. Cocke, T. Osipov, R. D. Muiño, H. Schmidt-Böcking, and R. Dörner, Nature (London) **431**, 437 (2004).
[5] J. S. Briggs and V. Schmidt, J. Phys. B: At., Mol. Opt. Phys. **33**, R1 (2000).
[6] G. Dawber, A. G. McConkey, L. Avaldi, M. A. MacDonald, G. C. King, and R. I. Hall, J. Phys. B: At., Mol. Opt. Phys. **27**, 2191 (1994).
[7] L. Avaldi and A. Huetz, J. Phys. B: At., Mol. Opt. Phys. **38**, S861 (2005).
[8] P. Franceschi, D. Ascenzi, P. Tosi, R. Thissen, J. Žabka, J. Roithová, C. L. Ricketts, M. D. Simone, and M. Coreno, J. Chem. Phys. **126**, 134310 (2007).
[9] T. Masuoka, Phys. Rev. A **48**, 1955 (1993).
[10] S. Hsieh and J. H. D. Eland, J. Phys. B: At., Mol. Opt. Phys. **29**, 5795 (1996).
[11] B. Gaire, S. Y. Lee, D. J. Haxton, P. M. Pelz, I. Bocharova, F. P. Sturm, N. Gehrken, M. Honig, M. Pitzer, D. Metz, H.-K. Kim, M. Schöffler, R. Dörner, H. Gassert, S. Zeller, J. Voigtsberger, W. Cao, M. Zohrabi, J. Williams, A. Gatton, D. Reedy, C. Nook, T. Müller, A. L. Landers, C. L. Cocke, I. Ben-Itzhak, T. Jahnke, A. Belkacem, and T. Weber, Phys. Rev. A **89**, 013403 (2014).
[12] J. H. D. Eland, S. D. Price, J. C. Cheney, P. Lablanquie, I. Nenner, and P. G. Fournier, Philos. Trans. R. Soc. London B **324**, 247 (1988).
[13] P. Lablanquie, J. H. D. Eland, I. Nenner, P. Morin, J. Delwiche, and M. J. Hubin-Franskin, Phys. Rev. Lett. **58**, 992 (1987).
[14] T. Ibuki, T. Imamura, I. Koyano, T. Masuoka, and C. E. Brion, J. Chem. Phys. **98**, 2908 (1993).
[15] G. Frenking, W. Koch, and H. Schwarz, J. Comput. Chem. **7**, 406 (1986).
[16] W. Koch, G. Frenking, F. Maquin, D. Stahl, and H. Schwarz, J. Chem. Soc. Chem. Commun. 1187 (1984).
[17] R. Dörner, V. Mergel, O. Jagutzki, L. Spielberger, J. Ullrich, R. Moshammer, and H. Schmidt-Böcking, Phys. Rep. **330**, 95 (2000).
[18] J. Ullrich, R. Moshammer, A. Dorn, R. Dörner, L. P. H. Schmidt, and H. Schmidt-Böcking, Rep. Prog. Phys. **66**, 1463 (2003).
[19] T. Jahnke, T. Weber, T. Osipov, A. L. Landers, O. Jagutzki, L. P. H. Schmidt, C. L. Cocke, M. H. Prior, H. Schmidt-Böcking, and R. Dörner, J. Electron Spectrosc. Relat. Phenom. **141**, 229 (2004).
[20] For details, visit www.roentdek.com.
[21] O. Jagutzki, V. Mergel, K. Ullmann-Pfleger, L. Spielberger, U. Spillmann, R. Dörner, and H. Schmidt-Böcking, Nucl. Instrum. Methods Phys. Res., Sect. A **477**, 244 (2002).
[22] O. Jagutzki, A. Cerezo, A. Czasch, R. Dörner, M. Hattaß, M. Huang, V. Mergel, U. Spillmann, K. Ullmann-Pfleger, T. Weber, H. Schmidt-Böcking, and G. D. W. Smith, IEEE Trans. Nucl. Sci. **49**, 2477 (2002).
[23] M. Krems, J. Zirbel, M. Thomason, and R. D. DuBois, Rev. Sci. Instrum. **76**, 093305 (2005).
[24] L. Malegat, F. Citrini, P. Selles, and P. Archirel, J. Phys. B: At., Mol. Opt. Phys. **33**, 2409 (2000).
[25] D. P. Seccombe, S. A. Collins, T. J. Reddish, P. Selles, L. Malegat, A. K. Kazansky, and A. Huetz, J. Phys. B: At., Mol. Opt. Phys. **35**, 3767 (2002).
[26] E. Sokell, P. Bolognesi, A. Kheifets, I. Bray, S. Safgren, and L. Avaldi, Phys. Rev. Lett. **110**, 083001 (2013).
[27] B. Brehm, U. Fröbe, and H. P. Neitzke, Int. J. Mass Spectrom. Ion Phys. **57**, 91 (1984).
[28] G. Frenking, W. Koch, M. Schaale, and H. Baumgärtel, Int. J. Mass Spectrom. Ion Phys. **61**, 305 (1984).
[29] G. Bieri, L. Åsbrink, and W. von Niessen, J. Electron Spectrosc. Relat. Phenom. **23**, 281 (1981).

[30] G. Bieri, W. von Niessen, L. Åsbrink, and A. Svensson, Chem. Phys. **60**, 61 (1981).
[31] J. L. Dehmer and D. Dill, Phys. Rev. A **18**, 164 (1978).
[32] K. Taylor, J. Phys. B: At. Mol. Phys. **10**, L699 (1977).
[33] S. Hara and M. Nakamura, J. Phys. B: At. Mol. Phys. **19**, L467 (1986).
[34] M. Alagia, C. Callegari, P. Candori, S. Falcinelli, F. Pirani, R. Richter, S. Stranges, and F. Vecchiocattivi, J. Chem. Phys. **136**, 204302 (2012).
[35] S. Hirokami and R. J. Cvetanović, J. Phys. Chem. **78**, 1254 (1974).
[36] E. M. Evleth and A. Sevin, J. Am. Chem. Soc. **103**, 7414 (1981).
[37] J. O'Reilly, S. Douin, S. Boyé, N. Shafizadeh, and D. Gauyacq, J. Chem. Phys. **119**, 820 (2003).
[38] A. H. H. Chang, A. M. Mebel, X.-M. Yang, S. H. Lin, and Y. T. Lee, J. Chem. Phys. **109**, 2748 (1998).
[39] J. van Tilborg, T. K. Allison, T. W. Wright, M. P. Hertlein, R. W. Falcone, Y. Liu, H. Merdji, and A. Belkacem, J. Phys. B: At., Mol. Opt. Phys. **42**, 081002 (2009).